INTERNATIONAL JOURNAL FOR NUMERICAL METHODS IN FLUIDS, VOL. 23, 1073–1084 (1996)

NUMERICAL SIMULATION OF THREE-DIMENSIONAL INCOMPRESSIBLE FLOW BY A NEW FORMULATION

C. J. HO AND F. H. LIN

Department of Mechanical Engineering, National Cheng Kung University, 70101, Tainan, Taiwan

SUMMARY

A new mathematical formulation, called the pseudovorticity–velocity formulation, of the three-dimensional incompressible Navier–Stokes equations is presented as an alternative to the vorticity–velocity approach. For the model lid-driven cavity flow problem in two and three dimensions, combined with an explicit mixed spectral/finite different numerical scheme the proposed formulation is found to be efficient and very accurate as compared with the results available in the literature. In particular, the simulation results demonstrate an attractive feature of the present formulation compared with the vorticity–velocity approach, namely that the divergence-free condition of the velocity field can always be achieved on a non-staggered mesh.

KEY WORDS: three-dimensional incompressible flow; lid-driven cavity flow; pseudovorticity–velocity formulation

1. INTRODUCTION

The mathematical formulations that are commonly used to simulate three-dimensional incompressible viscous flows include the primitive variables[1] (velocity–pressure), vorticity–vector potential[2,3] and vorticity–velocity[4] formulations. As indicated in an overview of these formulations by Gresho,[5] each formulation has its own advantages as well as shortcomings with respect to the others. Both the vorticity–vector potential formulations and the vorticity–velocity approach have a distinct advantage over the velocity–pressure formulation in that the pressure need not be calculated explicitly. The vorticity–velocity method, similar to the velocity–pressure formulation but unlike the velocity–vector potential approach, suffers from a major difficult in obtaining a solenoidal velocity field so that the continuity equation is satisfied explicitly. For the vorticity–velocity formulation the use of a staggered mesh or alternative boundary conditions for the vorticity has been proposed to provide a divergence-free velocity field.[6] In the velocity–vector potential formulation, however, the vector potential is not uniquely defined and a scalar potential is further required for the non-enclosed flow configuration.

It follows from the foregoing that it is highly desirable to develop a formulation having the advantages of the velocity–vorticity formulation but avoiding the difficulty of obtaining a divergence-free velocity field. Jia and Nakamura[7] recently presented a new formulation in terms of velocity and a new variable q for two-dimensional incompressible flow. It has been demonstrated that their formulation can be applied to both steady and unsteady flow simulations on a non-staggered grid, yielding an essentially divergence-free velocity field. The present study represents a continuing effort in pursuit of this aspect. In this paper we present a new formulation, called the pseudovorticity–velocity formulation, and its application to three-dimensional incompressible viscous flow

CCC 0271–2091/96/101073–12

Received November 1995
Revised March 1996

simulation. When applied to two-dimensional flow, the new formulation degenerates into the velocity–q formulation of Jia and Nakamura.[7] Therefore the present formulation can be viewed as the three-dimensional extension of their formulation. The three-dimensional flow in an upper-lid-driven cavity is used as a test problem for the new formulation developed.

2. PSEUDOVORTICITY–VELOCITY FORMULATION

The non-dimensional governing equations of laminar, incompressible flow of a Newtonian constant-viscosity fluid can be written as

$$\nabla \cdot \mathbf{V} = 0, \tag{1}$$

$$\frac{\partial \mathbf{V}}{\partial t} + (\mathbf{V} \cdot \nabla \mathbf{V}) = -\nabla p + \frac{1}{Re} \nabla^2 \mathbf{V}. \tag{2}$$

Here Re is the Reynolds number based on a characteristic length and a characteristic velocity of the flow: $\mathbf{V}$ and p denote the dimensionless velocity vector and the dimensionless pressure, respectively.

Taking the divergence of the incompressible Navier–Stokes equations (2) and applying the continuity equation (1) leads to a Poisson pressure equation of the form

$$\nabla \cdot [(\mathbf{V} \cdot \nabla \mathbf{V}) + \nabla p] = 0. \tag{3}$$

In order to satisfy equation (3) identically, a solenoidal vector $\tilde{\boldsymbol{\omega}}$ that satisfies

$$\nabla \times \tilde{\boldsymbol{\omega}} = (\mathbf{V} \cdot \nabla \mathbf{V}) + \nabla p \tag{4}$$

is introduced. Further, the viscous term in (2) can be recast as

$$\nabla^2 \mathbf{V} = \nabla(\nabla \cdot \mathbf{V}) - \nabla \times \boldsymbol{\omega} = -\nabla \times \boldsymbol{\omega}. \tag{5}$$

Here $\boldsymbol{\omega}(= \nabla \times \mathbf{V})$ is the dimensionless vorticity vector. The Navier–Stokes equations are then rewritten by applying equations (4) and (5):

$$\frac{\partial \mathbf{V}}{\partial t} + \nabla \times \left(\tilde{\boldsymbol{\omega}} + \frac{1}{Re} \boldsymbol{\omega} \right) = \mathbf{0}. \tag{6}$$

From (6) it can be noticed that the new variable $\tilde{\omega}$ is a vorticity-like quantity.

Next the governing equation for the new variable $\tilde{\boldsymbol{\omega}}$ is derived by first applying the curl operator to (4), i.e.

$$\nabla \times (\nabla \times \tilde{\boldsymbol{\omega}}) = \nabla \times [(\mathbf{V} \cdot \nabla)\mathbf{V} + \nabla p] = (\mathbf{V} \cdot \nabla)\boldsymbol{\omega} - (\boldsymbol{\omega} \cdot \nabla)\mathbf{V}. \tag{7}$$

Then, using the condition of a solenoidal vector for $\tilde{\boldsymbol{\omega}}$, i.e. $\nabla \cdot \tilde{\boldsymbol{\omega}} = 0$, the following relation is obtained as the governing equation for $\tilde{\boldsymbol{\omega}}$:

$$\nabla^2 \tilde{\boldsymbol{\omega}} = -(\mathbf{V} \cdot \nabla)\boldsymbol{\omega} + (\boldsymbol{\omega} \cdot \nabla)\mathbf{V} = \nabla \times (\mathbf{V} \times \boldsymbol{\omega}). \tag{8}$$

A new formulation for the three-dimensional incompressible flow simulation can then be expressed in terms of the velocity vector $\mathbf{V}$ and the new variable $\tilde{\boldsymbol{\omega}}$ governed by (6) and (8), respectively. In addition, taking the curl of (6) yields

$$\frac{\partial \boldsymbol{\omega}}{\partial t} = \nabla^2 \left(\tilde{\boldsymbol{\omega}} + \frac{1}{Re} \boldsymbol{\omega} \right). \tag{9}$$

From (9) the variable $\tilde{\boldsymbol{\omega}}$ can again be inferred to be a vorticity-like vector. Further, substituting equation (8) into (9), the following form of vorticity transport equation results:

$$\frac{\partial \boldsymbol{\omega}}{\partial t} + \nabla \times (\boldsymbol{\omega} \times \mathbf{V}) = \frac{1}{Re} \nabla^2 \boldsymbol{\omega}. \tag{10}$$

Note that under the steady flow condition, equation (9) reduces to

$$\nabla^2 \left(\tilde{\boldsymbol{\omega}} + \frac{1}{Re} \boldsymbol{\omega} \right) = \mathbf{0}, \tag{11}$$

which leads to

$$\tilde{\boldsymbol{\omega}} = -\frac{1}{Re} \boldsymbol{\omega} + \mathbf{C}. \tag{12}$$

In (12), $\mathbf{C}$ is an arbitrary constant vector and is taken to be a null vector for convenience. It can thus be inferred from (12) that for the present formulation under the steady flow condition the variable $\tilde{\boldsymbol{\omega}}$ is physically proportional but opposite in sign to the vorticity vector $\boldsymbol{\omega}$. Accordingly, the variable $\tilde{\boldsymbol{\omega}}$ can be viewed as a counterpart of the vorticity in the sense of rotation. The steady velocity field is a result of the balance between them. Hereinafter we will refer to the vorticity-like variable $\tilde{\boldsymbol{\omega}}$ as the 'pseudovorticity' or 'antivorticity' vector and the new formulation as the 'pseudovorticity–velocity' formulation.

Alternatively, the present formulation can be derived by first rewriting the vorticity transport equation (10), by means of the relations $\nabla \times (\nabla \times \boldsymbol{\omega}) = -\nabla^2 \boldsymbol{\omega}$ and $\boldsymbol{\omega} = \nabla \times \mathbf{V}$, in the form

$$\nabla \times \left(\frac{\partial \mathbf{V}}{\partial t} + \boldsymbol{\omega} \times \mathbf{V} + \frac{1}{Re} \nabla \times \boldsymbol{\omega} \right) = \mathbf{0}, \tag{13}$$

which leads to

$$\frac{\partial \mathbf{V}}{\partial t} + \boldsymbol{\omega} \times \mathbf{V} + \frac{1}{Re} \nabla \times \boldsymbol{\omega} = \nabla S. \tag{14}$$

In (14), mathematically, S is a scalar, while physically, $S = -(p + \frac{1}{2} \mathbf{V} \cdot \mathbf{V})$ by referring to the original Navier–Stokes equations (2). Further, taking the divergence of (14) and applying the continuity equation (1), we have

$$\nabla \cdot (\boldsymbol{\omega} \times \mathbf{V} - \nabla S) = 0. \tag{15}$$

Next, in order to have equation (15) hold identically, we assume a solenoidal vector $\tilde{\boldsymbol{\omega}}$ that follows

$$\nabla \times \tilde{\boldsymbol{\omega}} = \boldsymbol{\omega} \times \mathbf{V} - \nabla S. \tag{16}$$

Equation (6) is then obtained by substituting equation (16) into (14). Meanwhile, equation (8) can be obtained simply by taking the curl operator of (16).

Another interesting observation of the present formulation is that the pseudovorticity vector can be shown, as derived in the following, to be a linear combination of the vorticity and the time derivative of the vector velocity potential $\boldsymbol{\Phi}$, which is related to the velocity by the relation $\mathbf{V} = \nabla \times \boldsymbol{\Phi}$.

Substituting the relation $\mathbf{V} = \nabla \times \boldsymbol{\Phi}$ into (6) leads to

$$\nabla \times \left(\frac{\partial \boldsymbol{\Phi}}{\partial t} + \tilde{\boldsymbol{\omega}} + \frac{1}{Re} \boldsymbol{\omega} \right) = \mathbf{0}, \tag{17}$$

which implies that

$$\frac{\partial \Phi}{\partial t} + \tilde{\boldsymbol{\omega}} + \frac{1}{Re}\boldsymbol{\omega} = \mathbf{C}. \tag{18}$$

Under the steady flow condition, equation (18) reduces to (12).

Moreover, taking the divergence of (6) leads to

$$\frac{\partial(\nabla \cdot \mathbf{V})}{\partial t} = 0 \tag{19}$$

and thus $\nabla \cdot \mathbf{V} = \text{constant}$. This implies that the present formulation can effectively maintain the divergence-free condition as long as an initial divergence-free velocity field is used.

For two-dimensional flow the stretching term $(\boldsymbol{\omega} \cdot \nabla)\mathbf{V}$ in (8) vanishes together with $\boldsymbol{\omega} = \omega_k \hat{\mathbf{e}}_k$ and $\tilde{\boldsymbol{\omega}} = \tilde{\omega}_k \hat{\mathbf{e}}_k$, where $\hat{\mathbf{e}}_k$ is the unit vector normal to the flow plane. Accordingly, the form of (6) and (8) degenerates into a formulation identical with that of Jia and Nakamura[7]:

$$\frac{\partial \mathbf{V}}{\partial t} + \nabla\left(\tilde{\omega}_k + \frac{1}{Re}\omega_k\right) \times \hat{\mathbf{e}}_k = \mathbf{0}, \tag{20}$$

$$\nabla^2 \tilde{\omega}_k = -(\mathbf{V} \cdot \nabla)\omega_k. \tag{21}$$

It follows that the scalar variable q employed by Jia and Nakamura[7] is simply the component of the pseudovorticity vector normal to the flow plane, $\tilde{\omega}_k$.

The boundary conditions associated with the velocity equation (6) can be enforced straightforwardly by the given physical conditions of the velocity field under consideration. On the other hand, the boundary conditions for the pseudovorticity vector equation (8) can be derived utilizing the fact that the relation (12) also holds at the Dirichlet boundary condition and thus the boundary pseudovorticity can be treated in a similar manner to the vorticity on the boundary.

To validate the present formulation, the model problem of three-dimensional upper-lid-driven flow in a cubic cavity ($1 \times 1 \times 1$) is considered as shown in Figure 1.

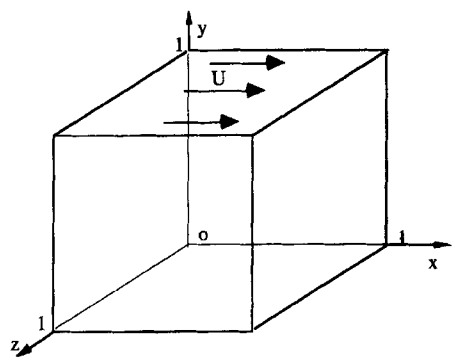

Figure 1. Flow configuration of three-dimensional upper-lid driven cavity flow

3. SOLUTION METHODOLOGY

The system of equation (6) and (8) is spatially discretized by applying a Chebyshev collocation method in the directions x and z and a second-order central finite difference scheme in the y-direction. The spectral discretization grids are given by the Gauss–Lobatto collocation points

$$x_i = \cos\left(\pi \frac{i}{I}\right), \quad i = 0, \ldots, I, \tag{22a}$$

$$z_k = \cos\left(\pi \frac{k}{K}\right), \quad k = 0, \ldots, K. \tag{22b}$$

A non-uniform finite difference grid distribution that provides denser grids near the boundaries is constructed via the scaled transformation

$$\eta = \frac{1}{2}\left(\frac{\tan(2y-1)\beta}{\tan\beta} + 1\right). \tag{23}$$

Here η is the transformed co-ordinate and β is the stretching degree. The mixed spectral/finite difference technique, as opposed to the pure spectral method, is employed here mainly owing to the fact that the finite difference scheme provides a better resolution of the strong velocity gradient in the y-direction near the constant-speed moving upper lid.

The time integration procedure is performed on the velocity equation (6) by means of an explicitly time discretization. Specifically, a three-level second-order Euler scheme is applied to replace the time derivative of the velocity vector, while the spatial derivative terms in (6) are evaluated using the second-order Adams–Bashforth scheme. In vector notation the time integration scheme adopted for the velocity equation can be expressed as

$$\frac{3\mathbf{V}^{n+1} - 4\mathbf{V}^n + \mathbf{V}^{n-1}}{2\Delta t} + \tfrac{3}{2}[\nabla \times (\tilde{\boldsymbol{\omega}} + \boldsymbol{\omega})]^n - \tfrac{1}{2}[\nabla \times (\tilde{\boldsymbol{\omega}} + \boldsymbol{\omega})]^{n-1} = \mathbf{0}, \quad n \geqslant 2, \tag{24}$$

where n denotes the time level. For the first time step the first-order explicit Euler time discretization is employed for the velocity equation.

The Poisson equations of the pseudovorticity $\tilde{\boldsymbol{\omega}}$ are solved using a preconditioned conjugate gradient iterative scheme Bi-CGSTAB-P[8] in which the matrix multiplication and the conjugate gradient method can be easily vectorized. This preconditioned iterative scheme is particularly efficient for the solution of the system of equations with non-symmetric matrices that the Chebyshev spectral collocation discretization always generates.

The solution procedure for the lid-driven cavity flow problem utilizing the pseudovorticity–velocity formulation starts with solving the Poisson equations of the pseudovorticity vector based on the initially/previously known vector field. The iterative computation for the pseudovorticity equations continues until a relative convergence criterion of 10^{-5} is achieved. Then the new velocity field is evaluated by solving the velocity equation in the form of (24). For a steady flow solution the above-described solution procedure is repeated until a steady state velocity field with an absolute convergence criterion of 10^{-6} is reached. To ensure the accuracy of the results, double precision is employed throughout the present simulations.

4. RESULTS OF TEST PROBLEM

Numerical simulations have been conducted using the mixed spectral/finite difference method for the upper-lid-driven flow in a cubic cavity at three values of the Reynolds number, $Re = 100$, 400 and 1000. Both two- and three-dimensional flow configurations are considered.

4.1. 2D square lid-driven cavity flow

First, results of the steady two-dimensional lid-driven flow are presented. As a result of a series of mesh convergence tests using various mesh systems, a 33 (x-direction) × 33 (y-direction) mesh system was selected for the cases of $Re = 100$ and 400 and a 41 × 41 mesh was used for $Re = 1000$. The time step used depends on Re: a time step of 0·001 for $Re = 100$ and 0·004 for $Re = 400$ and 1000. For each time step the CPU times required on an HP 715/75 workstation are about 0·13 s for the 33 × 33 mesh and 0·18 s for the 41 × 41 mesh. The steady lid-driven cavity flow structures obtained using the present formulation are illustrated by velocity vector plots and streamline contour maps in Figures 2 and 3, respectively. The computed flow structures are evidently in good qualitative agreement with the results of the existing literature.[1,9] Furthermore, Figure 4 presents the velocity profiles of the horizontal velocity component u at the cavity midplane and of the vertical velocity

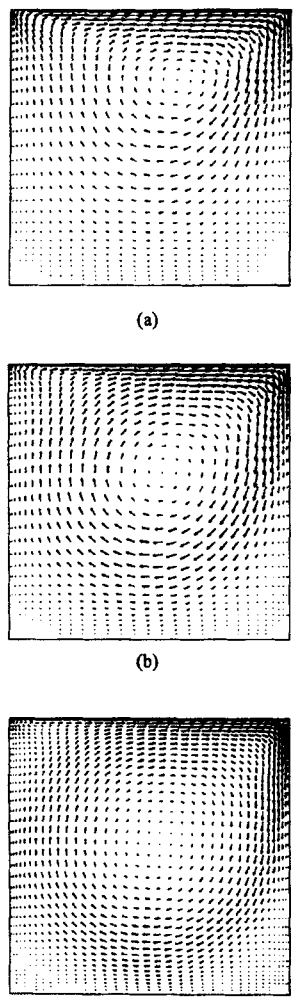

Figure 2. Velocity vectors for (a) $Re = 100$, (b) $Re = 400$ and (c) $Re = 1000$

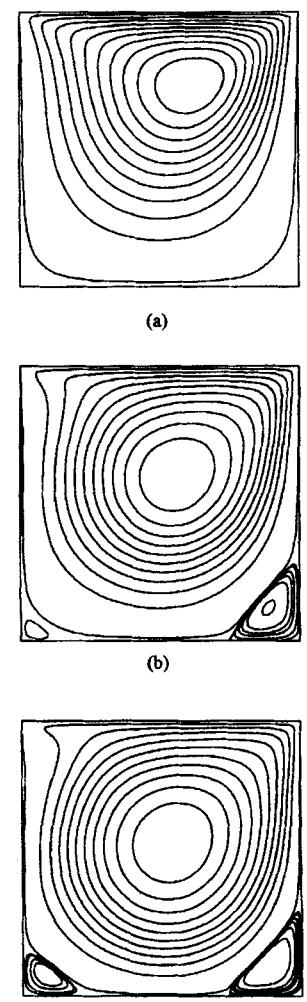

Figure 3. Streamline contours for (a) $Re = 100$, (b) $Re = 400$ and (c) $Re = 1000$

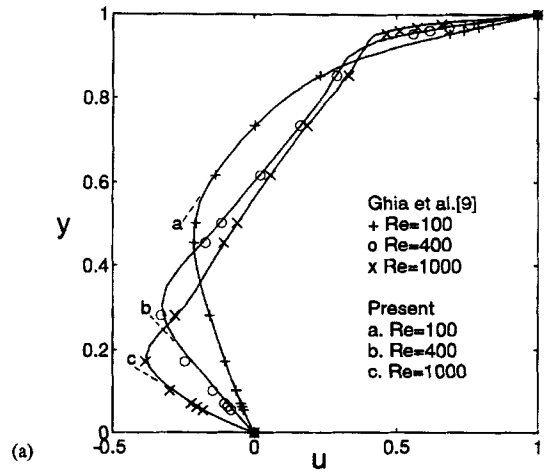

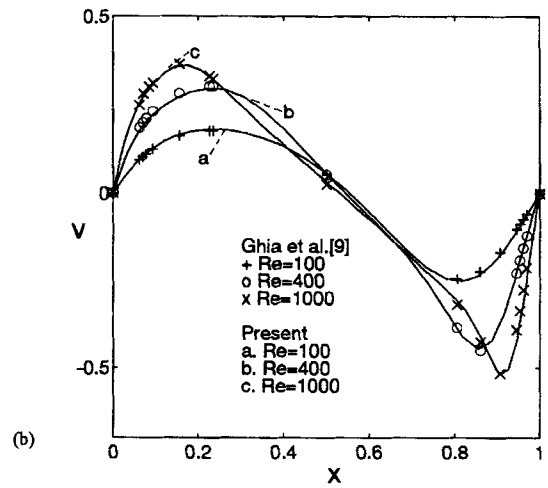

Figure 4. Velocity profiles on (a) vertical centrelines and (b) horizontal centreline

Table I. Comparison of location of primary vortex centre (x_c, y_c) and its streamfunction ψ_c and vorticity ω_c

	Present			Ghia *et al.*[9]			Ku *et al.*[1]
Re	(y_c, y_c)	ψ_c	ω_c	(x_c, y_c)	ψ_c	ω_c	ψ_c
100	(0·6154, 0,7368)	−0·1037	3·1670	(0·6172, 0·7344)	−0·1034	3·1665	−0·1037
400	(0·5550, 0·6078)	−0·1136	2·2951	(0·5547, 0·6055)	−0·1139	2·2947	−0·1137
1000	(0·5342, 0·5615)	−0·1161	2·0503	(0·5313, 0·5625)	−0·1179	2·0497	−0·1162

Table II. Maximum absolute value of velocity divergence for 2D and 3D lid-driven cavity flows

	$\lvert\nabla \cdot \mathbf{V}\rvert_{max}$	
Re	2D	3D
100	$9{\cdot}495 \times 10^{-13}$	$1{\cdot}243 \times 10^{-12}$
400	$5{\cdot}946 \times 10^{-13}$	$9{\cdot}500 \times 10^{-13}$
1000	$1{\cdot}020 \times 10^{-12}$	$1{\cdot}049 \times 10^{-12}$

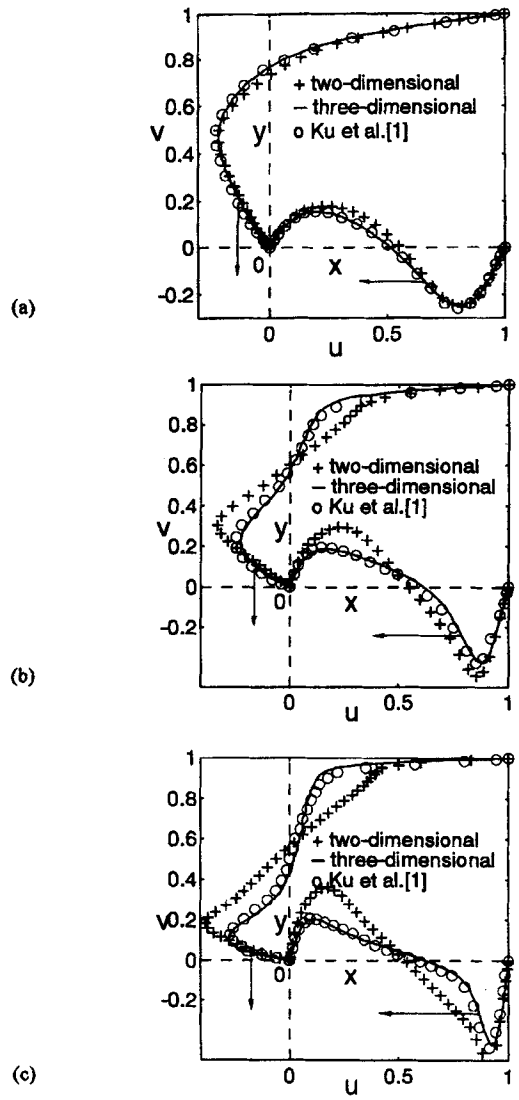

Figure 5. Velocity profiles on vertical and horizontal centrelines in z-symmetry plane for (a) $Re = 100$, (b) $Re = 400$ and (c) $Re = 1000$

component v at the horizontal midplane for the three values of Re. The predicted velocity profiles appear to agree very well with the results of Ghia *et al.*[9] that are also shown in the figure. In Table I we present a comparison of the results of the primary vortex centre locations as well as their streamfunction and vorticity with those obtained by Ghia *et al.*[9] and Ku *et al.*[1] It is clear that the results computed using the present formulation are in good agreement with the results obtained by the finite difference solutions of Ghia *et al.*[9] using a 129 × 129 mesh as well as with the pseudospectral solutions of Ku *et al.*[1] Another important aspect of the velocity fields computed using the present formulation is that the divergence-free condition can be essentially satisfied as demonstrated by Table II, in which the maximum absolute values of the velocity divergence ($\nabla \cdot \mathbf{V}$) for the three values of Re are listed. This provides further validation of the capability of the pseudovorticity–velocity formulation to yield an essentially divergence-free velocity field, in contrast with the standard vorticity–velocity approach.

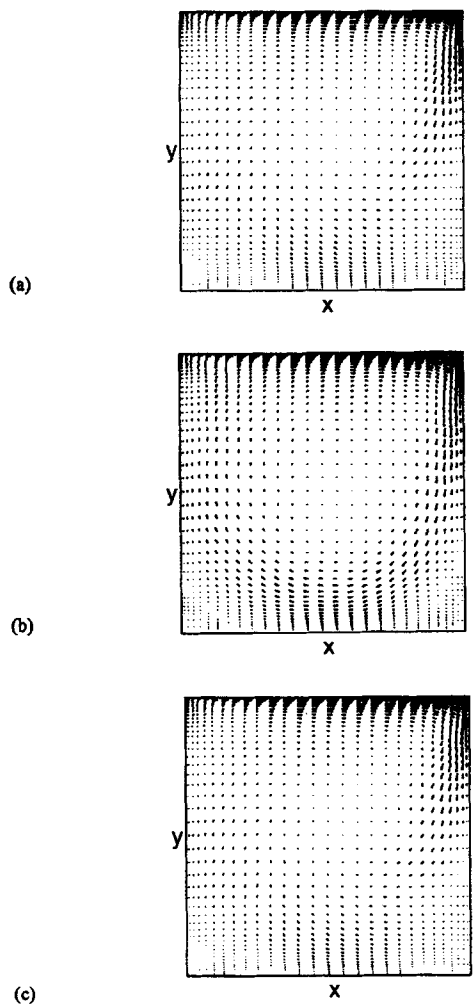

Figure 6. Flow direction vectors for $Re = 1000$ on (a) $z = 0{\cdot}043$ plane, (b) $z = 0{\cdot}5$ plane and (c) $z = 0{\cdot}957$ plane

4.2. 3D lid-driven cavity flow

Next, results from the simulation of the three-dimensional upper-lid-driven cavity flow using the present formulation will be presented. For the cases of $Re = 100$ and 400 a mesh of 25 (x-direction) $\times$ 41 (y-direction) $\times$ 25 (z-direction) was used, while for $Re = 1000$ a 31 $\times$ 47 $\times$ 31 mesh was found to be sufficiently fine. The time steps adopted for the calculations are 0·002 for $Re = 100$ and 0·008 for $Re = 400$ and 1000. Typically, the CPU time required for each time step using a mesh of 31 $\times$ 47 $\times$ 31 is 38·4 s on an HP 715/75 workstation. In Figure 5 the computed steady velocity profiles of u on the vertical centreline and v on the horizontal centreline of the symmetry plane (z=0·5) at $Re = 100$, 400 and 1000 are compared with the 3D predictions by Ku *et al.*[1] Also superimposed in Figure 5 are the computed results from our 2D simulations at the corresponding values of Re. Evidently, our predicted velocity profiles compare very well with the results of Ku *et al.*[1] In addition, similar to what was found in the previous study,[1] comparison of the velocity profiles

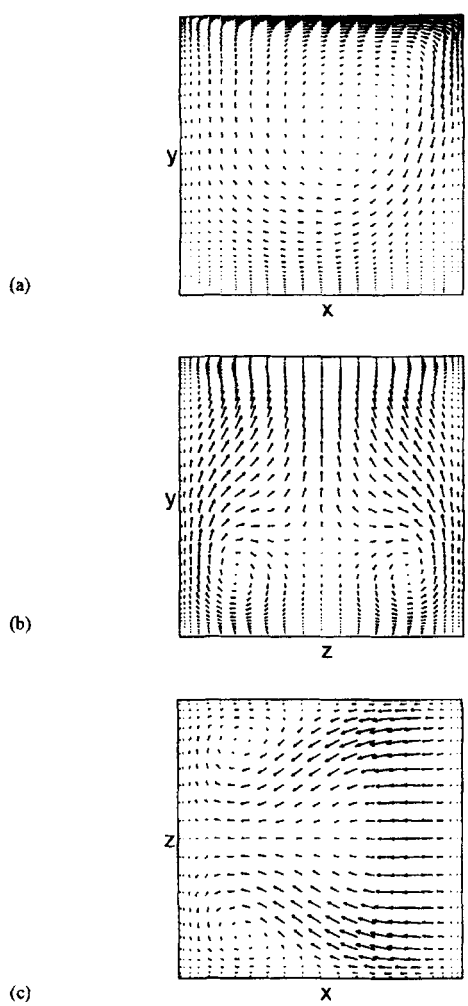

Figure 7. Flow direction vectors for $Re = 400$ on (a) $z = 0·5$ plane, (b) $x = 0·5$ plane and (c) $y = 0·5$ plane

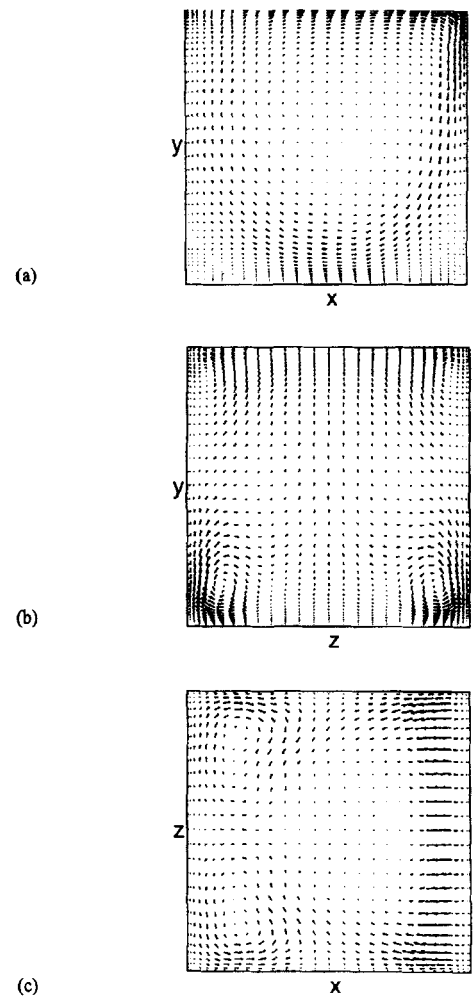

Figure 8. Flow direction vectors for $Re = 1000$ on (a) $z = 0·5$ plane, (b) $x = 0·5$ plane and (c) $y = 0·5$ plane

obtained from 2D and 3D simulations clearly demonstrates that the three-dimensional effect of the velocity profiles becomes increasingly distinctive with increasing Re. The three-dimensional effect can be further inferred from the disparity of the velocity vector plots at three x–y planes $z = 0{\cdot}043$, $0{\cdot}5$ and $0{\cdot}957$ shown in Figure 6 for $Re = 1000$. Moreover, Figures 7 and 8 display the velocity vector plots on three midplanes $x, y, z = 0{\cdot}5$ for $Re = 400$ and 1000 respectively. The symmetry of the velocity field with respect to the midplane $z = 0{\cdot}5$ can be readily detected from Figure 6. The velocity vector plots at the midplanes $x = 0{\cdot}5$ and $y = 0{\cdot}5$, shown in Figures 7(b) and 7(c) respectively, clearly illustrate the onset of contra-rotating transversal vortices, which strengthen with increasing Re and become more distinctive at $Re = 1000$ as displayed in Figures 8(b) and 8(c). The pair of contra-rotating vortices near the bottom corners of the midplane $y = 0{\cdot}5$, as displayed in Figures 7(c) and 8(c), tends to protrude towards the centre with increasing Re. Moreover, the pair of primary vortices on the plane $x = 0{\cdot}5$ is seen to shift towards the lower corners of the cavity as the Reynolds number is increased from 400 to 1000. Meanwhile, a pair of secondary vortices near the upper corners becomes increasingly discernible, as revealed in Figures 7(b) and 8(b). This has also been observed in previous studies.[10–12].

Finally, the velocity divergence of the computed three-dimensional velocity fields is evaluated and the maximum absolute values of the velocity divergence obtained are also presented in Table II. Again an essentially divergence-free velocity field is clearly achieved for the three-dimensional flow simulations using the present formulation, making it an attractive alternative to the vorticity–velocity approach.

5. CONCLUDING REMARKS

A new formulation in terms of the velocity vector and a pseudovorticity vector (pseudovorticity–velocity formulation) has been developed for solving the three-dimensional incompressible Navier–Stokes equations. The new variable, pseudovorticity, may be viewed as a counterpart of the vorticity in the sense of rotation. Numerical simulations using the pseudovorticity–velocity formulation combined with a mixed spectral/finite difference scheme have been undertaken for the 2D and 3D upper-lid driven cavity flow problems. The accuracy and efficiency of the proposed formulation have been demonstrated by the good agreement of the predicted results with those reported in the literature. In particular, the results have highlighted the attractive feature of the new formulation, in contrast with the vorticity–velocity approach, that an essentially divergence-free velocity field can always be obtained on a standard mesh. For two-dimensional flow the present formulation degenerates to the formulation proposed by Jia and Nakamura[7] and thus the present formulation can be viewed as its three-dimensional extension.

REFERENCES

1. H. C. Ku, R. S. Hirsh and T. D. Taylor, 'A pseudospectral method for solution of the three-dimensional incompressible Navier–Stokes equations', *J. Comput. Phys.*, **70**, 439–462 (1987).
2. K. Aziz and J. D. Hellums, 'Numerical solution of the three-dimensional equations of motion of laminar natural convection', *Phys. Fluids*, **10**, 314–324 (1967).
3. G. D. Mallinson and G. de Vahl Davis, 'Three-dimensional natural convection in a box: a numerical study', *J. Fluid Mech.*, **83**, 1–31 (1977).
4. S. C. R. Dennis, D. B. Ingham and R. W. Cook, 'Finite difference methods for calculating steady incompressible flows in three dimensions', *J. Comput. Phys.*, **33**, 325–339 (1979).
5. P. M. Gresho, 'Incompressible fluid dynamics: some fundamental formulation issues', *Ann. Rev. Fluid Mech.*, **23**, 413–453 (1991).
6. M. Napolitano and G. Pascazio, 'A numerical method for the vorticity–velocity Navier–Stokes equations in two and three dimensions', *Comput. Fluids*, **19**, 489–495 (1991).

7. W. Jia and Y. Nakamura, 'A new formulation for incompressible viscous flow', in Ch. Hirsch, J. Périaux and W. Kordulla. (eds), *Computational Fluid Dynamics* '92, Elsevier, Amsterdam, 1992, pp. 383–390.
8. H. A. Van der Vorst, 'Bi-CGSTAB: a fast and smoothly converging variant of BCG for the solution of nonsymmetric linear systems', *SIAM J. Sci. Stat. Comput.*, **13**, 631–644 (1990).
9. U. Ghia, K. N. Ghia and C. T. Shin, 'High-Re solutions for incompressible flow using the Navier–Stokes equations and a multi-grid method', *J. Comput. Phys.*, **48**, 387–411 (1982).
10. G. Guj and F. Stella, 'A vorticity–velocity method for the numerical solution of 3D incompressible flows', *J. Comput. Phys.*, **106**, 286–298 (1993).
11. S. Fujima, M. Tabata and Y. Fukasawa, 'Extension to three-dimensional problems of the upwind finite element scheme based on the choice of up- and downwind points', *Comput. Methods Appl. Mech. Eng.*, **112**, 109–131 (1994).
12. B. N. Jiang, T. L. Lin and L. A. Povinelli, 'Large-scale computation of incompressible Navier–Stokes equations by least-squares finite element method', *Comput. Methods Appl. Mech. Eng.*, **114**, 213–231 (1994).